

Abrasive Stripping Voltammetry and ESR Spectroscopy of Manganese in Carbonates

Šebojka Komorsky-Lovrić,^a Jens Bartoll,
Reinhard Stößer,* and Fritz Scholz*

*Institut für Chemie, Humboldt-Universität zu Berlin,
Hessische Str. 1–2, 10115 Berlin, Germany*

Received September 1, 1995; revised September 3, 1996; accepted October 16, 1996

A combined approach using solid state electroanalysis (abrasive stripping voltammetry) and ESR spectroscopy was made to characterize the different species of manganese which are present in natural and synthetic calcium carbonates. Abrasive stripping voltammetry permits identifying MnO_2 and MnCO_3 , but the method fails when it comes to detecting unambiguously MnCO_3 in the presence of MnO_2 . Neither can this method detect Mn^{2+} ions in mixed crystals of $\text{Ca}_{1-x}\text{Mn}_x\text{CO}_3$ because of their low concentrations. ESR spectroscopy can show that Mn^{2+} ions are present in calcite on Ca^{2+} sites. Additionally, information about the state and symmetry of Mn^{2+} sites and the local dynamics of the lattice can be obtained. In aragonite, only extremely small amounts of individual Mn^{2+} ions are present and most of the manganese is found in the form of MnO_2 agglomerates. Solid state electroanalysis and ESR spectroscopy allow a rather complete qualitative specification of manganese in calcium carbonates.

INTRODUCTION

A solid phase which is absolutely pure with respect to its chemical composition and physical structure is something that cannot exist. Impurities and imperfections are the natural constituents of every real solid phase. The lower their concentration, the more difficult it is to get information about

^a On leave from the Ruđer Bošković Institute, Zagreb, Croatia.

* Authors to whom correspondence should be addressed.

the state of impurities. Therefore, every method is welcome which promises to give access to information on impurities, be it chemical or physical. In the present paper, we intend to show that very conventional electrochemical measuring techniques and ESR spectroscopy provide complementary information allowing a description of the state of impurities.

Solid state electroanalysis is a rapidly developing field of research,¹ which has got a strong impetus by the development of an electrode preparation technique in which the sample is mechanically immobilized on the surface of a suitable, in most cases a graphite electrode^{2,3} (so-called abrasive stripping voltammetry).

We have extended our systematic studies of solid compounds to metal ions immobilized in inert matrices. The immobilization of foreign metal ions in a host matrix is a very common case in many natural systems. If a solid phase is precipitated from a solution, foreign ions will be co-precipitated. Very well-known systems are iron oxide-hydrates precipitating from rivers, lakes and the sea. The characterization of such co-precipitates is not a trivial task. The first question arising is whether the foreign ions form a separate solid phase.* The second question is the size of these separate phase particles and how small they may be to be still regarded as a separate phase. Then, it is important to know the location of this separate phase. Is it an inclusion in the host crystals or is it a surface coverage (two-dimensional?) of the major component? Is it in the adsorbed state? Do the ions of the microcomponent substitute those of the major component in their crystal lattice (solid solution)? All these questions cannot be answered by any existing physicochemical technique alone. However, using a combination of different techniques, it is possible to get an insight into the complex situation of impurities.

In the present communication, we describe the electrochemistry of the microcomponents Mn^{2+} , Mn^{4+} in the macrocomponent $CaCO_3$. In the subsequent part, we shall describe the electrochemistry of other metal ions, such as Pb^{2+} , Ag^+ and Cu^{2+} in inert matrices like $Mg(OH)_2$. These are all model systems, which have been chosen to study the capabilities of electrochemical methods.

Solid state electroanalysis, esp. abrasive stripping voltammetry, is applicable to the identification of separate phases^{4,5} and also to the identification and analysis of mixed crystals, *i.e.* solid solutions. Examples of the abrasive stripping voltammetric analysis of mixed crystals are $AgCl_{1-x}Br_x$,⁶ $Cu_2Se_{1-x}S_x$ and $CuBi_{1-x}Sb_xS_2$.⁷ From the analysis of these mixed crystals we know that AbrSV is not applicable to the detection of less than 1% of the minor constituent. This limitation exists because, at such a low concentration, the potential shift of the signal is too small to be reliably distinguishable from the natural scattering of results. Fortunately, it is below 1% that the range of

* »Phase« should not be understood in its pure thermodynamic meaning, but there are also precursors of different kinds and solid solutions considered.

concentration starts where ESR spectroscopy is especially useful as the interaction of the paramagnetic centres with each other becomes negligible and well-resolved spectra are obtainable.

In the case of solid solutions, the electrochemical signal shifts continuously from one border value to the other according to the thermodynamics of mixed phases. In the case of two separate phases, one obtains two separate signals. ESR spectroscopy can probe the atomic environment of a foreign paramagnetic ion in the diamagnetic crystalline or non-crystalline matrix or that of the solid solution. However, it will most probably fail when it comes to detecting separate phases of the paramagnetic species due to extensive spin-coupling. Although the presence of a paramagnetic phase may be detected from its influence on the spectra of the paramagnetic species, which are present in the adjacent diamagnetic phase, electrochemical measurements give a much easier and more reliable access to the detection of such a phase, provided it possesses electrochemical activity. In co-precipitations of Mn^{2+} (minor constituent) and Ca^{2+} (major constituent) with carbonate ions, one can at least expect the following phases: CaCO_3 , $\text{Ca}_{1-x}\text{Mn}_x\text{CO}_3$ ($x \ll 1$), MnCO_3 , MnO_2 . The formula MnO_2 is used here to describe the rather complex manganese(III, IV)-oxide-hydrates. CaCO_3 can neither be detected by electrochemistry nor by ESR spectroscopy. X-ray diffraction is the method of choice for its characterization. For $\text{Ca}_{1-x}\text{Mn}_x\text{CO}_3$, ESR spectroscopy will be the best method, esp. in the cases where $x \ll 1$. MnCO_3 and MnO_2 are accessible by AbrSV, provided that the absolute amount of the compound immobilized on the electrode surface exceeds 10^{-11} mol, since this is the detection limit.⁸

Electron Spin Resonance (ESR) is a powerful tool for the investigation of paramagnetic centres in solids.⁹⁻¹¹ Organic or inorganic radicals as well as transition metal ions are often used as »reporters« with regard to the structure and dynamics of the local co-ordination sphere in solids.

In the present case of manganese-doped CaCO_3 , information on the oxidation state, aggregation, symmetry of the paramagnetic centre and its diamagnetic environment should be accessible.¹²

Only Mn^{2+} ions are directly observable by ESR in CaCO_3 . A strong Jahn-Teller-distortion in the case of Mn^{3+} effects an extreme line broadening. Mn^{4+} signals will only be detected if individual centres occur, but Mn^{4+} shows a great tendency to form MnO_2 or its precursors. However, manganese ions present in higher oxidation states can influence the relaxation behaviour of Mn^{2+} ions.

There are five unpaired electrons in Mn^{2+} ions, so we find a ^6S -ground state. Hyperfine interaction of the unpaired electrons with the manganese nucleus ($I = 5/2$) causes a characteristic hyperfine splitting. The hyperfine interaction shows similar strength as the electron spin – electron spin interaction, i.e. zero field splitting (zfs).¹³⁻¹⁶

EXPERIMENTAL

Instrumentation

Voltammetric measurements were performed with an AUTOLAB (ECO-Chemie, Utrecht, Netherlands) in conjunction with an electrode stand VA 663 (Metrohm, Switzerland) and a personal computer (IBM compatible 386DX33-PC).

The X-band spectra were recorded with an ESR spectrometer of type ESR 300 (Zentrum für wissenschaftlichen Gerätebau, Berlin, Germany) at temperatures of 300 K, 77 K, 300–1200 K (Bruker high-temperature equipment) and 4 K (APD Cryogenics USA). Quartz tubes of 3 mm diameter were used.

Chemicals

Preparation of the Solid Phases

(i) $\text{Mn}^{2+}/\text{CaCO}_3$. 20 ml of a 1 M CaCl_2 solution was added dropwise to 200 ml of a 0.1 M Na_2CO_3 solution (a) at room temperature to get calcite and (b) at 55 °C to get aragonite. The calcium chloride solution was spiked with appropriate amounts of MnCl_2 to get coprecipitates. In this way pure calcite and aragonite containing about 10% calcite were obtained. Furthermore, natural calcite and aragonite samples from the collection of our department were used (see Table I). The samples are available on the request.

(ii) MnCO_3 was freshly precipitated by the standard procedure.¹⁷ MnO_2 was electrodeposited from an acidic MnSO_4 solution using the recommended procedure.¹⁸ Only analytical-grade chemicals (all »Merck«) were used.

Electrochemical Measurements

Small amounts (a few mg) of the solid compound are placed on a clean glazed porcelain tile. The lower circular surface of a paraffin-impregnated graphite rod electrode (PIGE) is gently rubbed on the compound spot to transfer the sample onto the electrode surface. The PIGEs are made by impregnation of graphite rods with melted paraffin (m.p. 65 °C) under vacuum. The graphite rods are the same as the electrodes used in the spectrographic emission analysis. A detailed description of PIGEs and the abrasive transfer technique is published elsewhere.²

A platinum gauze was the counter electrode and an $\text{Ag}/\text{AgCl}/3 \text{ M KCl}$ (Metrohm) was the reference electrode ($E = 0.208 \text{ V vs. SHE}$).¹⁹ The supporting electrolyte was 1 M KNO_3 (Merck, analytical grade). Water was double distilled. Solutions were degassed with high-purity nitrogen for 30 min prior to measurements. A nitrogen blanket was maintained thereafter. The cell was thermostated at 20 °C.

RESULTS AND DISCUSSION

Abrasive Stripping Voltammetry

Electrochemically, manganese oxides and oxyhydroxides have been investigated extensively because of the importance of these oxides for the manufacturing of batteries.^{20–23} Besides, analytical procedures based on the

reduction of electrochemically accumulated MnO_2 ^{24–26} or the redox reaction of Mn(II) ions^{27,28} have been developed.

Figure 1 shows a cyclic voltammogram ($dE/dt = 100$ mV/s) of MnO_2 , which was mechanically transferred to the surface of a paraffin-impregnated graphite electrode (PIGE) by abrasion. A starting potential is 0 V and the initial scan direction is negative. The voltammogram is characterized by peaks I–IV. In the first cycle, the peak of the reduction at -0.5 V and the one of the oxidation at $+1$ V are enhanced. It is well known that MnO_2 contains a certain amount of Mn(III) ions.^{21–23} So, the peak marked I can be attributed to the reduction of Mn(III) to Mn(II) , while the reoxidation of Mn(II) to Mn(III) occurs at $+0.2$ V (peak II).^{22,27} The reduction of Mn(II) ions does not occur at potentials more positive than -1.4 V.²⁸ The pair of peaks III and IV most probably corresponds to the oxidation of Mn(III) to Mn(IV) and to the rereduction of Mn(IV) to Mn(III) .^{23–26} In the second and subsequent cycles, the assumed reduction of Mn(III) occurs at -0.2 V.

Abrasive cyclic voltammograms of MnCO_3 are shown in Figure 2. They are also characterized by peaks I–IV, but with additional peak IIb at $+0.5$ V, which appears in the second cycle and gradually disappears in the subsequent cycles while peak IIa increases.

The assignment of peak IIb is uncertain. In the first cycle, there are no peaks marked by I and IIb. It has also to be considered that peak IIa is very low while peak III is very high. This can be explained by the assumption that there are no Mn(III) ions in the freshly prepared MnCO_3 . So, there is no reduction of Mn(III) to Mn(II) at -0.5 V (peak I). Also, under these conditions, Mn(II) is not oxidized to Mn(III) (peaks IIa and IIb), but directly to Mn(IV) (peak III). A similar direct oxidation is used for the accumulation of Mn^{2+} ions.^{24–26} So, in the first cycle, the difference between the cyclic voltammograms of MnO_2 and MnCO_3 is the reductive peak I. This is a consequence of the difference in the contents of Mn(III) in these two precipitates.

For analytical purposes, it is convenient to combine the abrasive transfer of powders with the square-wave stripping voltammetry, which is shown to be very sensitive to traces of metal ions immobilized at the working electrode surface.^{29,30}

After the abrasive transfer of MnO_2 or MnCO_3 , the electrode was kept charged to the starting potential during 60 s in the electrolyte (1 M KNO_3), which was stirred to oxidize or to reduce Mn(III) ions. The abrasive stripping square-wave voltammograms of MnO_2 and MnCO_3 are shown in Figures 3–6. The voltammograms depend on the starting potentials, which were either $+1.5$ V or -1.5 V.

Figure 3A shows the SWV of MnO_2 , with the starting potential being $+1.5$ V. It consists of three peaks at $+0.95$ V, -0.35 V and -0.75 V, respectively. The first peak, at $+0.95$ V, is almost reversible, as it can be seen from the forward and the backward components of SWV responses, which are

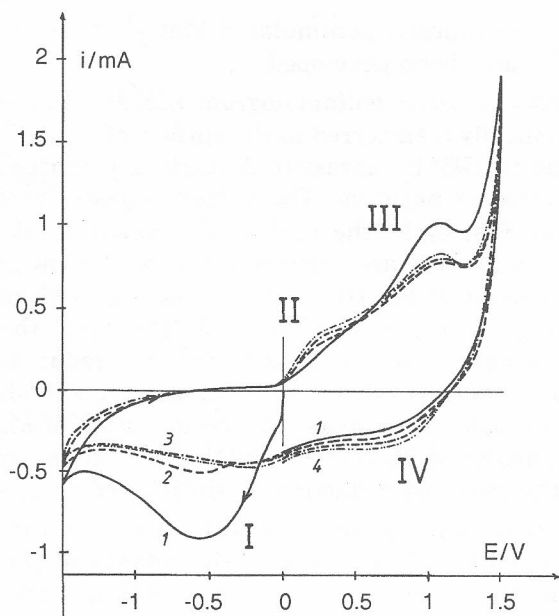


Figure 1. Abrasive cyclic voltammetry of MnO_2 in 1 M KNO_3 . Initial scan from 0 V to -1.5 V. $dE/dt = 100$ mV/s.

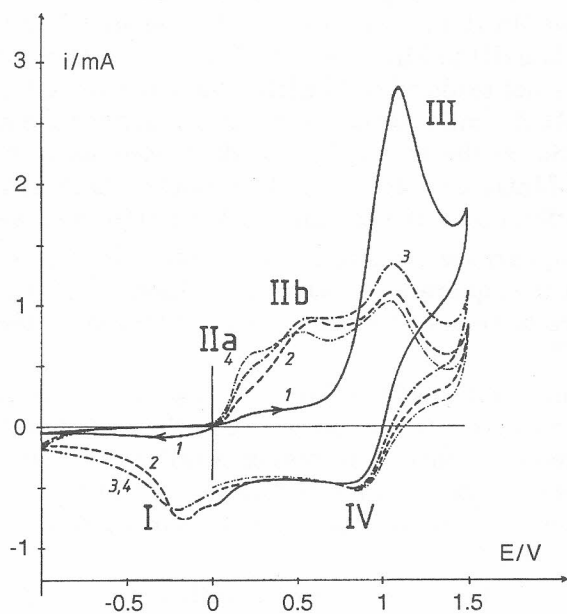


Figure 2. Abrasive cyclic voltammetry of MnCO_3 in 1 M KNO_3 . Initial scan from 0 V to -1.5 V. $dE/dt = 100$ mV/s.

shown in Figure 3B. This figure shows that the other two peaks are totally irreversible. The first peak probably corresponds to the reduction of Mn(IV) to Mn(III), and the other two to the reduction of Mn(III) to Mn(II).

If the starting potential is -1.5 V, the SWV of MnO_2 will exhibit only one peak at $+1$ V which is quasi reversible, as it can be seen in Figures 4A and 4B. Between 0 V and $+0.5$ V, there is a sign of a lower, irreversible peak which is covered by the much higher peak at $+1$ V. Such response is probably the consequence of the stepwise oxidation of the Mn(II) to Mn(III) and Mn(IV).

The square-wave voltammogram of MnCO_3 , as recorded from the starting potential of $+1.5$ V, also exhibits only one broad peak at $+0.62$ V and the sign of a lower peak at about $+0.2$ V (see Figure 5). Both peaks are reversible, as it can be seen in Figure 5B. They can be attributed to the re-reduction of Mn(IV), which was created by the oxidation of Mn(II) at $+1.5$ V during 60 s. The oxidation of MnCO_3 can be seen in Figures 6A and 6B. The starting potential is -1.5 V and the square-wave voltammogram exhibits two peaks: a very small one at $+0.06$ V and a big one at $+1$ V. Both peaks are totally irreversible. This is similar to the response of MnO_2 under the same conditions.

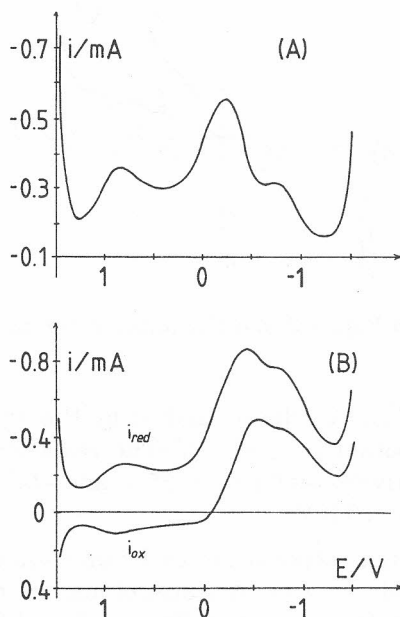


Figure 3. Abrasive stripping square-wave voltammetry of MnO_2 in 1 M KNO_3 . (A) Net response. (B) Forward (1) and backward (2) components of the response. Initial potential $+1.5$ V, $f = 8$ Hz, $\alpha = 50$ mV and $t_{\text{acc}} = 60$ s.

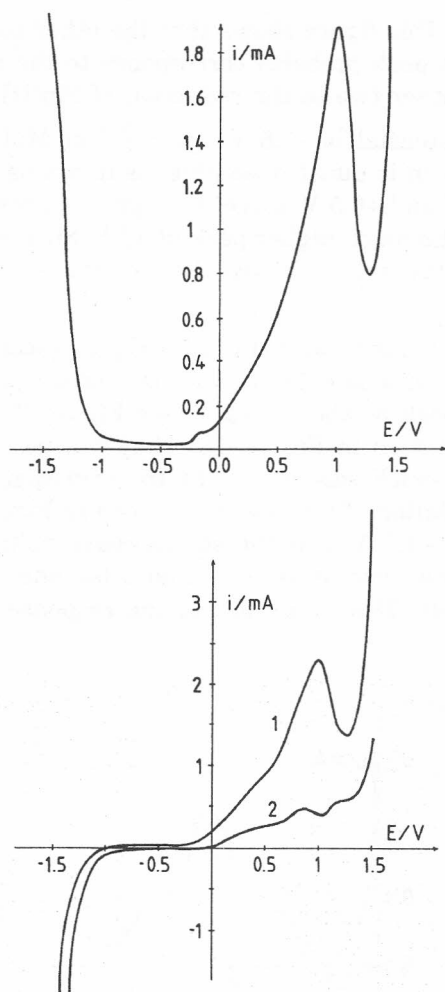


Figure 4. The same as in Figure 3, but the initial potential is -1.5 V.

MnO_2 and $MnCO_3$ can be distinguished by the square-wave voltammogram if the starting potential is $+1.5$ V. The response of MnO_2 consists of three peaks at, respectively, $+0.95$ V, -0.35 V and -0.75 V, while $MnCO_3$ exhibits only one peak at $+0.6$ V.

The differences in the responses of cyclic and square-wave voltammetry can be used for the analysis of redox states of manganese impurities in mineral samples. An example is shown in Figures 7 and 8. A sample of calcite, containing 0.008% Mn, was analyzed by abrasive cyclic voltammetry and the result is shown in Figure 7. In the first cycle, a well developed peak at about -0.4 V can be noted. This peak exists in the second and all subsequent cy-

cles. The peak marked II in Figure 1 can also be recognized as well as peak IV, but peak III is not well-developed. However, the appearance of peak I in the first cycle indicates the presence of Mn(III) in the sample. This is confirmed by the square-wave voltammogram shown in Figure 8A. It consists of three peaks at +0.98 V, -0.15 V and -0.75 V, respectively. The last two peaks are totally irreversible (Figure 8B). Although the peak potentials do not match the response of MnO_2 exactly, we can assume that the sample contains manganese, which is partly found in the form of Mn(III), while the

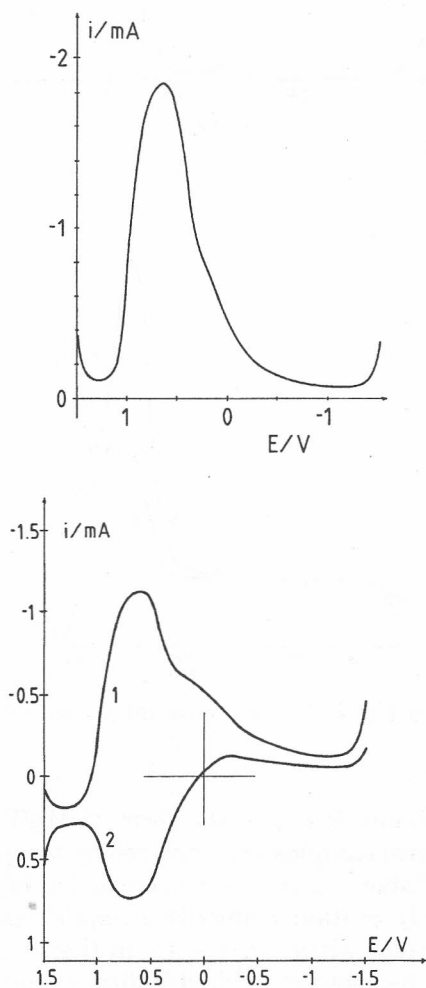


Figure 5. Abrasive stripping square-wave voltammetry of MnCO_3 in 1 M KNO_3 . (A) Net response. (B) Forward (1) and backward (2) components of the response. Initial potential +1.5 V. All other data as in Figure 3.

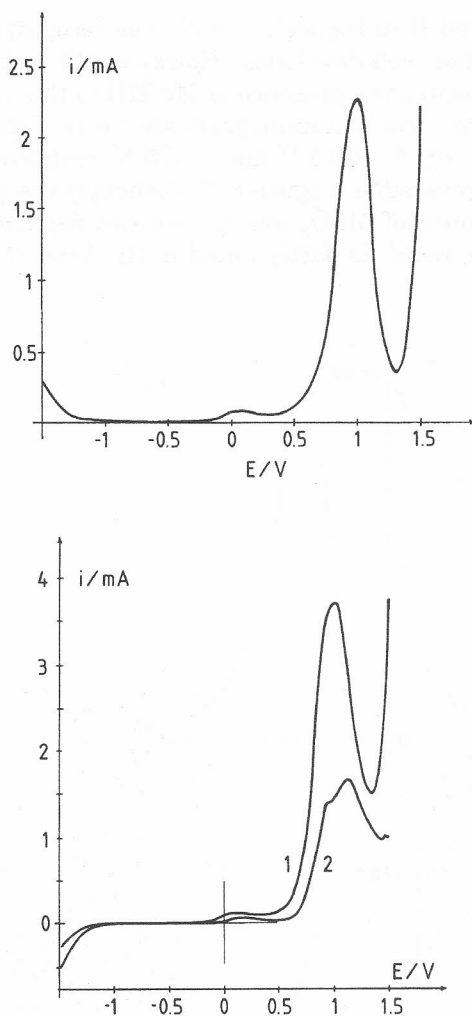


Figure 6. The same as in Figure 5, but the initial potential is -1.5 V.

rest of it is most probably found in the form of Mn(IV), as in the case of MnO_2 . The other mineral samples are analyzed by the same method and the results are shown in Table I. The general conclusion is that all investigated minerals most probably contain manganese impurities as separate phases or as precursors of phases which are mostly in the 4+ oxidation state. It is, however, a fact that the method applied indicates the presence of Mn(III) in the sample and not the presence of Mn(IV) or Mn(II). It is only the fact that the presence of Mn(III) is more likely to be associated with the presence of Mn(IV) than with Mn(II) that permits us to draw such a conclusion.

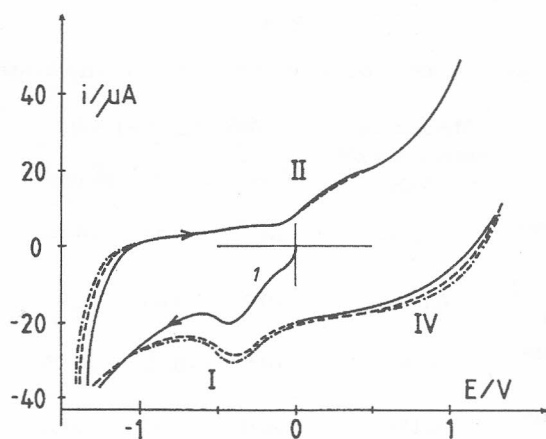


Figure 7. Abrasive cyclic voltammery of the sample of precipitated calcite, with the manganese content, $w \times 100$, being 0.008 (AAS). Initial scan from 0 V to -1.5 V. $dE/dt = 100$ mV/s. Supporting electrolyte 1 M KNO_3 .

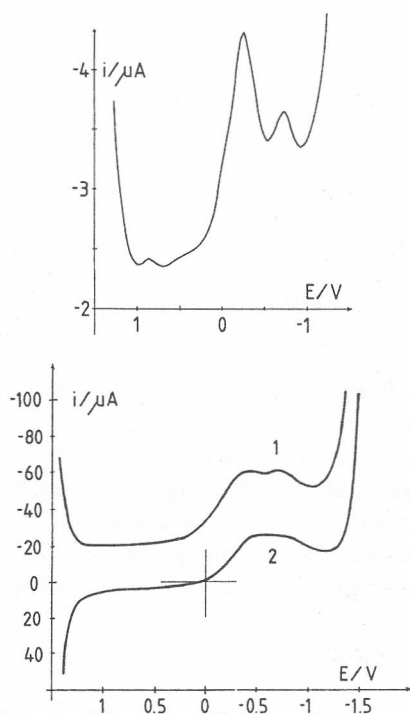


Figure 8. Abrasive stripping square-wave voltammery of the same sample as in Figure 7. Supporting electrolyte 1 M KNO_3 . (A) Net response. (B) Forward (1) and backward (2) components of the response. Initial potential $+1.5$ V. All other data as in Figure 3.

TABLE I

Electrochemical signals observed in different natural and synthetic samples

Sample	Manganese content, $w \times 100$ (AAS)	SWV ($E_{st} = +1.5$ V)			CV	
		$(E_p)_{I/V}$	$(E_p)_{II/V}$	$(E_p)_{III/V}$	$(E_p)_{I/V}$	$(E_p)_{II/V}$
natural black aragonite Spain	0.0009	+0.9	-0.35	-0.75		
natural aragonitic snail shell (<i>Helix pomatia</i>)	0.0013	+0.9	-0.40	-0.65	-	-
precipitated aragonite (about 10% calcite)	0.05	+0.9	-0.35	-0.75	-0.4	-
precipitated aragonite (about 10% calcite)	0.138	+0.9	-0.35	-0.75		
natural white calcite	?	+0.95	-0.42	-0.72		
natural pink calcite Mexico	0.01	+0.95	-0.40	-0.75		
precipitated calcite	? <0.008	-	-0.26	-	-0.4	-
precipitated calcite	0.008	+0.98	-0.15	-0.75	-0.45	+0.2
precipitated calcite	0.03	+0.9	-0.25	-	-0.3	+0.15
precipitated calcite	0.06	+0.9	-0.37	-0.75	-	-
precipitated calcite	0.914	+1.0	-0.25	-	-	+0.2

SWV: $f = 8$ Hz
 $a = 50$ mV
 $t_{acc} = 60$ s

CV: $dE/dt = 100$ mV
 $E_i = 0$ V
initial scan negative

ESR Spectroscopy

Manganese in Calcite

As shown in Figure 9, the manganese-doped calcite (see Table I) exhibits the typical ESR pattern frequently observed in samples containing calcite.^{12,15,16,31-38} Acceptably resolved spectra can only be obtained if the magnetic interactions between the Mn^{2+} ions are small as compared with the fine and hyperfine interactions inside the individual Mn^{2+} coordination polyhedra. Under these circumstances, the spectra can be completely simulated by a homemade computer program using the following spin-hamiltonian:^{9,32}

$$H = g\beta BS + ASI + D(S_z^2 - 1/3 S^2) + E(S_x^2 - S_y^2).$$

The simulation of the experimental spectrum (Figure 9b) reproduces the latter completely (Figure 9c) and yields parameters $g = 2,000$, $A = 2,618$ MHz and $D = 240$ MHz. This small zero-field-splitting (zfs) of approximately 2.5% of the microwave energy used in the x-band ESR experiments accounts for only

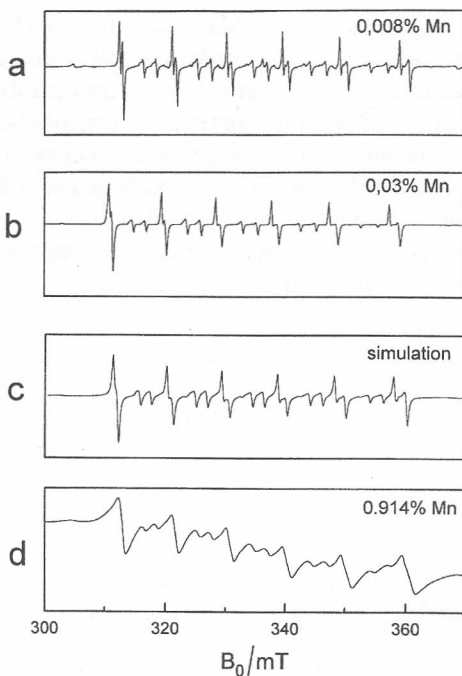


Figure 9a-d. ESR powder spectra of precipitated calcite doped with different quantities of manganese II. (Room temperature, x-band) and simulation.

slightly distorted lattice positions occupied by the Mn^{2+} ions. Therefore, $\text{Mn}^{2+} \rightarrow \text{Ca}^{2+}$ substitution must be taken into account. The magnetic interactions between the Mn^{2+} ions and between Mn^{2+} and other magnetic ions present in the samples (e.g. Mn^{3+} , Mn^{4+} , Fe^{2+} , and Fe^{3+} ions) result in line-broadening effects, as shown in Figure 9d. Barbin *et al.*³³ pointed out that such effects occur in samples containing manganese above the concentration range of ≈ 800 ppm. Summarizing the known experimental facts concerning Mn-doped calcite, it is, on principle, no problem to reproduce the spectra by simulation. This is true if the concentration of the Mn and other magnetic species is low and no internal tensions (e.g. strain) or similar phenomena are present.

Manganese in Aragonite

In nature, aragonite mostly occurs as a component of shells, corals or other biological carbonate products. As Figure 10 shows, the ESR pattern of natural aragonite (here it is the snail shell of *Helix pomatia*) differs remarkably from that of calcite (Figure 9). In both cases, the ESR response originates from Mn^{2+} ions. As it can be seen from Figure 10, the simulation

with parameters $g = 2,000$, $A = 2,620$ MHz, $D = 660$ MHz and $E = 150$ MHz covers only the main features of the experimental spectrum. The latter contains even further coexisting Mn^{2+} and other paramagnetic species. They are governed by other degrees of local distortions in comparison to the main part of the Mn^{2+} ions considered in the simulation process. Therefore, the complex experimental spectrum is not only an evidence of a higher degree of local distortion of the Mn coordination polyhedra due to the larger zero field splitting. It also indicates the enlarged structural degrees of freedom in the aragonite, as compared with calcite.

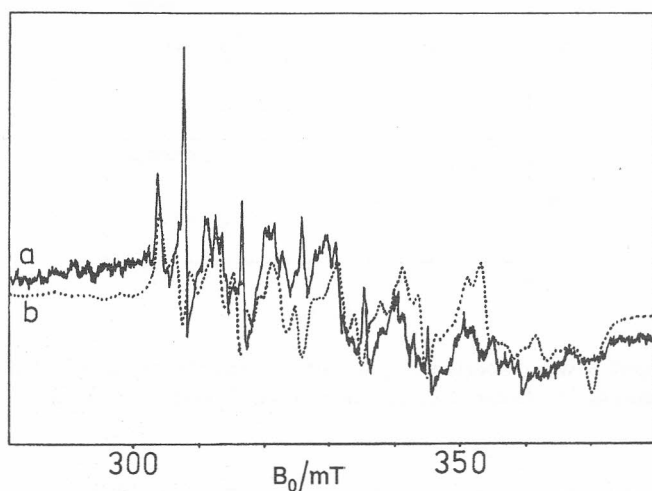


Figure 10. ESR powder spectrum of aragonitic snail shell (*Helix pomatia*) (room temperature, x-band). (—) experimental and (· · ·) simulated spectra.

Rhodochrosite (MnCO_3) forms a calcite-type lattice, as well. In calcite, the Ca^{2+} or Mn^{2+} ions are surrounded by oxygen atoms forming an almost perfect octahedron. In aragonite, these ions are ninefold coordinated. This type of coordination can lead to a lower local symmetry. On the other hand, the coordination polyhedron built of nine oxygen atoms bears more degrees of freedom and, therefore, allows incorporation of relatively large cations like Sr^{2+} , Ba^{2+} and Pb^{2+} ions. The carbonates of these ions build up an aragonite-like lattice. However, the ionic radius of Mn^{2+} is comparatively small. Therefore, Mn^{2+} ions will not prefer a special site in the coordination polyhedron representing a structural unit in the aragonite lattice. Similar phenomena were described also for Perovskite-type lattices.³⁴

As a result, there is a distribution of the spin-hamiltonian parameters^{10,32} and, together with stronger interactions of Mn^{2+} with neighbouring

ions, complex ESR spectra appear. From this point of view, it is not surprising that very different statements about the ESR of manganese in aragonite could be found in the literature.^{31,35-38} Obviously, there are both instrumental and material reasons for the non-unique interpretation of the ESR of aragonites. This situation induced further investigations in this field, starting originally from studies performed on snail shells. For example, in crystalline black aragonites (Spain) and other old geochemically formed aragonites only very small ESR signals were detected. Furthermore, it was necessary to use crystals instead of powders and carry out the measurements at 4.2 K. In contrast, aragonitic shells and other geologically young aragonites like »Sprudelstein« from a recent spring in Karlovy Vary (Czech Republic) and even samples freshly precipitated in the laboratory show relatively intensive Mn^{2+} signals. It means that one of the reasons for the small ESR signal of old aragonite minerals results from long oxidation and aggregation processes. The individual Mn^{2+} ions will be transformed into MnO_2 phases or into its precursors while these processes are in action. Obviously, the specifics of the structure of aragonite favours this kind of redox processes. Therefore, the presence of manganese in higher oxidation states is not surprising if, for example, coprecipitates of Ca^{2+} and Mn^{2+} with carbonate ions are formed under laboratory conditions without any exclusion of oxygen. In all the cases, only combinations of analytical methods were discussed, as it is done here with electrochemical and ESR techniques, and it is possible to provide information about the nature and the interactions of different manganese species existing in an actual sample. Evidence for manganese ions in higher oxidation states can also be given by high-temperature ESR equipment. Here, the appearance of the typical ESR pattern for individual Mn^{2+} ions at higher temperatures indicates this dissociation and reorganization of MnO_x aggregates. This corresponds well to the findings of the electrochemical measurements by which MnO_2 phases in the samples investigated are discovered.

From thermal analysis, it is well-known that aragonite transforms to calcite in the range of 500 °C. Figure 11 shows the ESR response starting with a sample of black natural aragonite (Spain) which was transformed thermally at 600 °C in different atmospheres into calcite. Samples heated in an H_2 atmosphere yield here the most intensive Mn^{2+} signals which are, for example, 2.6 times higher than those treated in air. Finally, it could be stated that an O_2 atmosphere affects the Mn^{2+} signals to a much lesser extent, *i.e.* about 60% of the intensity remains with respect to the samples treated in air. It means the equilibrium between the Mn^{2+} and Mn^{4+} ions present in the samples will be shifted by $p(O_2)$ for the benefit of Mn^{4+} in MnO_2 -like phases. Additionally, the signals of free radicals and electronic defects detected in the central part of the spectra obtained under the influence of a N_2/H_2 or air atmospheres, respectively, were quenched by the reaction with oxygen. Consequently, the experiments using reducing or oxidizing at-

mospheres support the presumption that the main part of manganese in aragonites of high geological ages occurs in higher oxidation states for thermodynamic reasons.

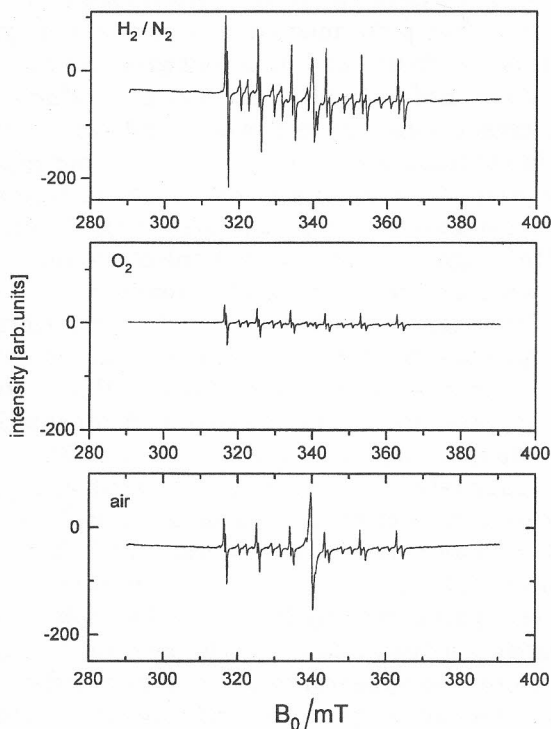


Figure 11. ESR powder spectra of an originally aragonite (transformed to calcite) thermally treated at 600 °C in different atmospheres (room temperature, x-band).

Saturation Behaviour and Spin Relaxation

As shown by simulations, the ESR spectral pattern of Mn^{2+} point defects is mainly governed by fine and hyperfine splittings. When powder samples are investigated, detailed structural information cannot be extracted from the values of these splittings. The analysis of the relations between the intensities of the allowed and forbidden transitions, on the one hand, and the saturation behaviour of the transitions, on the other hand, can give a deeper insight into the local structure and its dynamics. Structural information up to the identification of different manganese containing paramagnetic centres was obtained by Boughriet *et al.*³⁸ performing a careful analysis of the spectra.

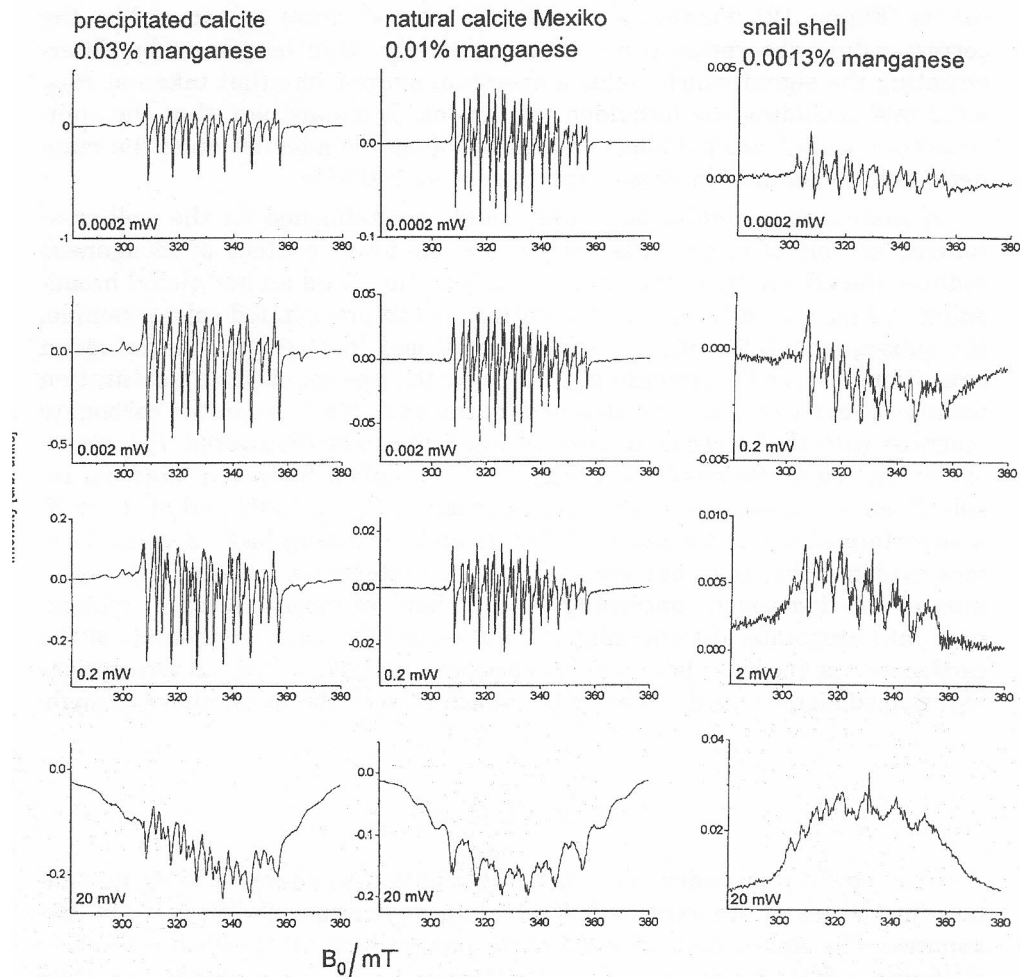


Figure 12. ESR powder spectra of carbonates measured at different levels of microwave power (4 K, x-band).

A distinct response of the spin systems to the enlarged microwave power applied (P_{MW}) is expected at low temperatures (4.2 K). As Figure 12 shows, the spectra of the precipitated calcite containing 0.03% manganese give specific responses to the microwave power. Up to $P_{MW} = 0.2$ mW, the ratio between the allowed and forbidden transitions tends to enlarge. The forbidden transitions with $\Delta m_I \neq 0^9$ concern the lines appearing between the ^{55}Mn -hyperfine sextet. They indicate the magnitude of the zfs including the distributions of D and E caused by internal tensions. Enlarging P_{MW} up to 20 mW saturation broadening becomes relevant in the sample of the precipitated

calcite (Figure 12). Furthermore, passage effects⁹ cause a pattern like the corresponding absorption curve. This statement could be proven by differentiating the signal which yields a spectrum shaped like that taken at $P_{MW} = 0.2$ mW including the forbidden transitions. It means here that the spin-relaxation times⁹ are not short enough to follow the modulation of the magnetic field performed in these experiments at 100 kHz.

A qualitatively similar behaviour could be established for the well crystallized sample of calcite (Mexico), where the lower content of manganese reduces the effectivity of the spin-spin interactions and an additional broadening at $P_{MW} = 20$ mW results. In contrast to the precipitated calcite sample, the subsequent differentiation of the signal does not resolve the forbidden transitions ($\Delta m_I \neq 0$). Accordingly, by using the low-temperature saturation technique, even very small differences of the spin dynamics in the carbonate matrices with their specific degrees of freedom can be discovered. Inspection of the spectra of the snail shell (Figure 12) reveals a further interesting result. Even by comparison of the spectra taken at $P_{MW} = 0.002$ and at 0.2 mW, a superimposition of spectra of different and coexisting Mn^{2+} species becomes evident. This is in agreement with the statements given at the beginning of the discussion concerning the problems of incorporation of manganese into aragonite. Additionally, the influence of organic compounds of the carbonate matrix must be taken into account. At higher P_{MW} , an absorption-like shaped signal was detected again, which showed the usual phase, though.

CONCLUSIONS

This study was undertaken as a contribution to characterizing manganese in species of different oxidation numbers incorporated in calcium carbonates. The application of solid state electrochemical analysis (abrasive stripping voltammetry) and ESR spectroscopy allowed a rather complete qualitative specification of manganese in synthetic and natural samples of $CaCO_3$. The electrochemical analysis provides an unambiguous evidence of the presence of MnO_2 phases. However, it fails when it comes to detecting $MnCO_3$ in the presence of MnO_2 and $Ca_{1-x}Mn_xCO_3$ for $x < 0.01$. The latter mixed crystals were studied by ESR spectroscopy with the following results:

(i) If there are low concentrations (<300 ppm) of manganese in the calcite samples, individual Mn^{2+} centres are found.

(ii) Manganese is probably situated on Ca^{2+} sites. The lattice seems to show a certain tolerance towards small distortions.

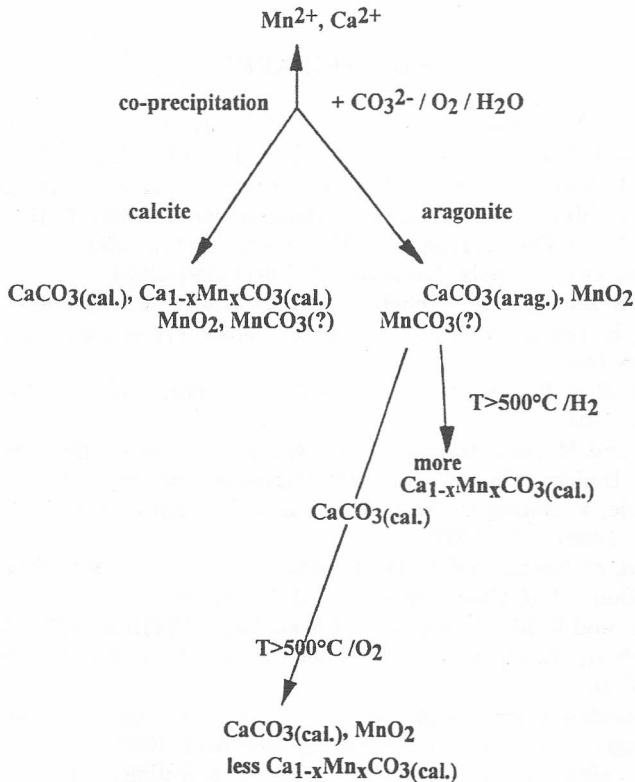
(iii) If there are higher concentrations, manganese oxygen aggregates will be observed. Under these conditions, the forming of aggregates should decrease the total energy of the lattice, since larger parts of the lattice are only slightly or not at all distorted.

(iv) The manganese spectra of aragonite reflect structural specifics of the aragonite. However, the main part of manganese is not situated on individual Ca^{2+} sites of aragonite.

(v) There are different ESR-active concentrations of Mn^{2+} in aragonite samples, depending on formation and age. The Mn^{2+} content in aragonite decreases with time by the reaction with oxygen. Since Mn^{2+} ions are not stabilized in the aragonite matrix over a long period of time, it is reasonable to assume the presence of MnCO_3 aggregates. MnCO_3 is known to be oxidized by oxygen during long time spans, which leads to the formation of MnO_2 aggregates. In contrast, it will be much more difficult to oxidize individual Mn^{2+} ions localized on Ca^{2+} sites in a calcite lattice.

(vi) The increase of ESR detectable Mn^{2+} after thermal treatment in an H_2 atmosphere in comparison with the treatment in an O_2 atmosphere gives evidence of the existence of manganese in more than two oxidation states in the aragonite samples investigated.

The following scheme summarizes the main results of this study:



Scheme 1

The results obtained are in general agreement with what is known about the geochemistry of manganese.³⁹ The formation of MnO_2 in the course of co-precipitation of Mn^{2+} and Ca^{2+} with a carbonate solution is a result of the alkaline pH of the carbonate solution. Thus, a competition occurs between the precipitation of CaCO_3 , $\text{Ca}_{1-x}\text{Mn}_x\text{CO}_3$, MnCO_3 , and $\text{Mn}(\text{OH})_2$. The latter is known to be rapidly oxidized by ambient oxygen to MnO_2 , which is the basis of the well-known Winkler-titration of oxygen. MnCO_3 is rather stable, but can be converted to MnO_2 in geological time spans if oxygen and water are present. $\text{Ca}_{1-x}\text{Mn}_x\text{CO}_3$ is most probably very stable provided that the host lattice is calcite. Mn^{2+} doping of aragonite is obviously less likely to occur as the Mn^{2+} ions do not fit very well into the Ca^{2+} sites of the aragonite lattice. In the case of aragonite precipitation, most of the manganese forms MnO_2 and possibly also MnCO_3 .

Acknowledgement. – Š. Komorsky-Lovrić gratefully acknowledges the International Bureau of the KfA, Jülich, for a Visiting Scholarship to Humboldt University. Additionally, the authors acknowledge support by Deutsche Forschungsgemeinschaft and Fonds der Chemischen Industrie.

BIBLIOGRAPHY

1. F. Scholz and B. Meyer, *Chem. Soc. Rev.* **23** (1994) 341–347.
2. F. Scholz and B. Lange, *Trends Anal. Chem.* **11** (1992) 359–367.
3. F. Scholz, L. Nitschke, and G. Henrion, *Naturwissenschaften* **76** (1989) 71.
4. S. Zhang, B. Meyer, G. Moh, and F. Scholz, *Electroanalysis* **7** (1995). 319–328.
5. B. Meyer, Ph.D. Thesis, Humboldt University, Berlin, 1995.
6. A. M. Bond and F. Scholz, *Langmuir* **7** (1991) 3197–3204.
7. B. Meyer, S. Zhang, and F. Scholz, *Fresenius J. Anal. Chem.* **356** (1996) 267–270.
8. F. Scholz, B. Lange, A. Jaworski, and J. Pelzer, *Fresenius J. Anal. Chem.* **340** (1991) 140–144.
9. J. A. Weil, J. R. Bolton, and J. Wertz, *Electron Paramagnetic Resonance*, Wiley, New York, 1994.
10. R. Stößer and M. Nofz, *Glastechn. Ber. Glass Sci. Technol.* **67** (1994) 156–165.
11. J. Bartoll, Diploma Thesis, Humboldt University, Berlin, 1994.
12. Lj. Brečević, V. Nöthig-Laslo, D. Kralj, and S. Popović, *J. Chem. Soc., Faraday Trans.* **92** (1996) 1017–1022.
13. F. K. Hurd, M. Suchs, and W. D. Hershberger, *Phys. Rev.* **93** (1954) 373–377.
14. H. M. McConnell, *J. Chem. Phys.* **24** (1956) 904–905.
15. C. Kikuchi and L. M. Matarrese, *J. Chem. Phys.* **33** (1960) 601–606.
16. G. E. Barberis, R. Calvo, H. G. Maldonado, and C. E. Zarate, *Phys. Rev. B* **12** (1975) 853–860.
17. *Gmelin Handbuch der Anorganischen Chemie*, 8. Auflage, C7, System-Nr. 56, pp. 174, Springer-Verlag, Berlin-Heidelberg-New York, 1981.
18. *Gmelin Handbuch der Anorganischen Chemie*, 8. Auflage, C1, System-Nr. 56, pp. 157, Springer-Verlag, Berlin-Heidelberg-New York, 1973.
19. U. Tinner, *Elektroden in der Potentiometrie*, Metrohm, Herisau, 1989, p. 16.

20. C. C. Liang, in: A. J. Bard (Ed.), *Encyclopedia of Electrochemistry of Elements*, Vol. I, Marcel Dekker, New York, 1973, p. 349–403.
21. F. L. Tye, in: B. Schumm, R. L. Middaugh, M. P. Grotheer, and J. C. Hunter (Eds.), *Manganese Dioxide Electrode Theory and Practice for Electro-chemical Applications*, The Electrochem. Soc., London, 1985, p. 301–341.
22. D. Y. Qu, L. Bai, C. G. Castledine, B. C. Conway, and W. A. Adams, *J. Electroanal. Chem.* **365** (1994) 247–259.
23. B. A. Lopez de Mishima, T. Ohtsuka, and N. Sato, *Electrochim. Acta* **38** (1993) 341–347.
24. E. Hrabankova, J. Dolezal, and V. Ma, *J. Electroanal. Chem.* **22** (1969) 195–201.
25. Y. Zhang, K. Jiao, C. Liu, and X. Liu, *Anal. Chim. Acta* **282** (1993) 125–132.
26. J. Labuda, M. Vanickova, and E. Beinrohr, *Mikrochim. Acta* (Vienna) 1989, I, 113–120.
27. F. Nakashima, *Anal. Chim. Acta* **30** (1964) 167–175.
28. R. J. O'Halloran and H. Blutstein, *J. Electroanal. Chem.* **125** (1981) 261–271.
29. M. Lovrić, Š. Komorsky-Lovrić, and A. M. Bond, *J. Electroanal. Chem.* **319** (1991) 1–18.
30. Š. Komorsky-Lovrić, M. Lovrić, and A. M. Bond, *Anal. Chim. Acta* **258** (1992) 299–305.
31. J. Lech and A. Šlezak, *Chem. Phys. Lett.* **157** (1989) 175–179.
32. N. Steinfeld, Ph.D. Thesis, Humboldt University, Berlin, 1995.
33. A. El Ali, V. Barbin, G. Calas, B. Cervelle, K. Ramseier, and J. Bouroulec, *Chem. Geol.* **104** (1993) 189–197.
34. I. D. Brown, *Acta Crystallogr., Sect. B* **48** (1992) 553–572.
35. W. Low and S. Zeira, *Am. Mineral.* **57** (1972) 1115–1131.
36. L. K. White, A. Szabo, P. Carkner, and N. D. Chasteen, *J. Phys. Chem.* **81** (1977) 1420–1424.
37. I. Lech, A. Šlezak, and I. Bojko, *Phys. Stat. Sol. (b)* **126** (1984) 371–380.
38. A. Boughriet, B. Ouddane, and M. Wartel, *Mar. Chem.* **37** (1992) 149–169.
39. R. Seim and G. Tischendorf, *Grundlagen der Geochemie*, VEB Deutscher Verlag für Grundstoffindustrie, Leipzig, 1990, p. 370.

SAŽETAK

Abrazivna voltametrijia otapanja i ESR spektroskopija mangana u karbonatima

Šebojka Komorsky-Lovrić, Jens Bartoll, Reinhard Stößer i Fritz Scholz

Tragovi iona mangana u prirodnim i sintetskim kristalima kalcijeva karbonata analizirani su elektrokemijski i spektroskopski. Uporabljene su dvije metode: voltametrijia s abrazivnim nanošenjem čestica krutih elektrolita na površinu grafitne elektrode (Abr. SV) i spektroskopija spinske rezonancije (ESR). Elektroanalitičkom metodom moguće je razlikovati izdvojene faze $\text{MnO}_2(\text{s})$ i $\text{MnCO}_3(\text{s})$, ali joj je osjetljivost premalena da bi se registrirali izolirani ioni Mn^{2+} u miješanim kristalima $\text{Ca}_{1-x}\text{Mn}_x\text{CO}_3$. ESR spektroskopijom moguće je dokazati prisutnost iona Mn^{2+} na mjestima kalcija u CaCO_3 i analizirati simetriju naboja oko iona Mn^{2+} i dinamiku kristalne rešetke. Tragovi mangana u aragonitu većinom su u obliku aglomerata MnO_2 .